Process Safety and Environmental Protection 141 (2020) 321–332

Contents lists available at ScienceDirect

Process Safety and Environmental Protection

journal homepage: www.elsevier.com/locate/psep

Insight into simultaneous catalytic oxidation of benzene and toluene in air over the nano-catalyst: Experimental and modeling via CFD-ANN hybrid method

Amin Sokhansanj, S. Majid Abdoli, Mohammad Zabihi *

Chemical Engineering Faculty, Sahand University of Technology, P.O. Box 51335-1996, Sahand New Town, Tabriz, Iran

ARTICLE INFO

Article history:
Received 2 April 2020
Received in revised form 15 May 2020
Accepted 18 May 2020
Available online 29 May 2020

Keywords:
Oxidation
Metal organic framework
Computational fluid dynamic
Neural network

ABSTRACT

This study reveals the simultaneous deep oxidation of benzene and toluene over the novel supported cobalt oxide catalyst derived from metal organic framework (MOF) over the almond shell based activated carbon. The performance of the fabricated catalyst was evaluated under the various operating conditions including oxidation temperature, initial concentration of benzene and toluene. The maximum conversion of benzene and toluene were also measured to be 89.74 % and 82.37 %, respectively. The sample morphology was studied by applying XRD, FESEM, BET and TGA analysis. The characterization tests indicated that the well dispersed spherical nano-supported catalyst was synthesized with size of less than 40 nm. To the best of our knowledge, the computational fluid dynamics (CFD) analysis incorporated with artificial neural network (ANN) was also studied for modeling the deep catalytic oxidation over the prepared sample. The modeling involved with the three dimensional analysis of polluted air flow through of a tubular micro-reactor axial inlet and outlet. The computational fluid dynamics was coded by adopting COMSOL Multiphysics to model the catalytic conversion of volatile organic compounds (VOCs) inside the porous media. The kinetic modeling was also conducted by using three-layer ANN to determine the reaction rates while the reaction temperature, initial concentration of benzene and toluene were considered as the input variables of network. The reaction rates were calculated by a non-linear feed-forward network with 5 neurons and log-sigmoid function in the hidden layer while the correlation coefficient was achieved to be 0.99. The validation of CFD model was accomplished which showed the appropriate matching between the experimental data and model achievements. Therefore, the developed intelligent hybrid model (CFD-ANN) in the offered investigation can be a useful tool for studying the fluid dynamics of VOCs oxidation over the nano-catalyst under the different operating conditions.

1. Introduction

Presence of the volatile organic compounds (VOCs) in the exhausted gas of many industrial factories causes the various health and environmental problems (Azalim et al., 2010; Jeon and Jeon, 2017; Tidahy et al., 2007a). In the meantime, benzene, toluene, and xylene (BTX) known as priority pollutants by the U.S environmental protection agency (EPA) are the major VOCs that have similar physical and chemical properties with highly toxic and carcinogenic specification (Montero-Montoya et al., 2018). Therefore, the removal and the separation of the mentioned compounds are of particular importance.

Among the various techniques (Anjum et al., 2019; Bandura et al., 2017; Binas et al., 2019; Derco et al., 2017; Jafari et al., 2018; Lee et al., 2020; Li et al., 2018; Liang et al., 2015; Lu et al., 2020; Rajamanickam et al., 2020), catalytic oxidation is one of the most significant methods for the removal of BTX compounds from the air (Deng et al., 2018; Pham et al., 2019; Russo et al., 2018). Bimetallic nanoparticles are applied as the efficient catalysts for the deep oxidation of VOCs in the presence of oxygen which has been investigated recently (Fiorenza et al., 2015; Li et al., 2020a; Nowicka and Sankar, 2018; Tabakova et al., 2015). Cobalt as the available and the low cost metal has been employed as an active site for the total oxidation of VOCs in many offered works (Choya et al., 2020; Łojewska et al., 2009; Todorova et al., 2020, 2019; Zhao et al., 2020). The various substrates activated carbon (Zabihi et al., 2015), alumina (Hyodo et al., 2015; Sedjame et al., 2014) and zeolite (Popova et al., 2019; Tidahy et al., 2007b) have been also used

* Corresponding author.
E-mail address: zabihi@sut.ac.ir (M. Zabihi).

https://doi.org/10.1016/j.psep.2020.05.035
0957-5820/

for the preparation of the supported metal oxides in the oxidation of VOCs process. Activated carbon due to its high surface area and proper catalytically performance would be in the central focus of researches.

In the recent years, the metal oxide catalysts have been synthesized from the metal organic framework (MOF) materials as a template to prepare the modified structure of nano-catalysts (Li et al., 2020b). The coating activated carbon by metal organic framework can be an appropriate by-material for the formation of arranged monometallic and bimetallic catalysts for the complete oxidation of VOCs. Cobalt oxide catalyst was fabricated from the metal organic framework template for the conversion of toluene in the air at the low temperature in the range of 150−300 °C (Liu et al., 2015). The Co-MOF was calcined at about 325 °C for preparation the cobalt oxide catalyst. Mn-Co bimetallic oxide was synthesized by using metal organic framework formation with different molar ratios of Mn and Co for total oxidation of VOCs (Luo et al., 2018). The well dispersed uniform metal oxide with high valence of surface was characterized by using various tests. Polyhedron cobalt oxide with different sizes was prepared from ZIF-67 for the deep combustion of toluene in the air (Zhao et al., 2019). The results showed that the complete oxidation of toluene was carried out at temperature in the range of 200−280 °C. CO oxidation was evaluated by using cobalt oxide catalyst derived from ZIF-67 by thermal treatment (Chen et al., 2020).

In addition to experimental studies, modeling strategies have been developed to investigate the behavior of chemical processes. Computational fluid dynamics (CFD) is increasingly being used to predict a behavior of the chemical reactor for the catalytic oxidation process. Da Costa et al. (2003), and Bounaceur et al. (2005) individually investigated and modeled benzene and toluene oxidation in a jet-stirred reactor. The detailed kinetic mechanism to reproduce their experimental results was proposed in these studies. The catalytic oxidation of vanillic acid in the trickle bed reactor was modeled by Lopes et al. (Lopes et al., 2007). Based on the generalized kinetic model, the kinetic parameters were obtained and the CFD design equations have been solved using user-defined routines in the commercial software Fluent. The CFD results showed a significant temperature effect, whereas the partial pressure of the air had only a minor influence. Niaei et al. (Niaei et al., 2008) studied the gas catalytic oxidation of ethyl acetate over Cr-HZSM-5 catalyst. Two-stage Redox kinetic model (known as the Mars van Krevelen model) was used to explain the catalytic oxidation of VOC and Fluent v. 6.2 was utilized in this catalytic process simulation. The findings indicate elevated temperatures and low inlet mass flow rate boost the conversion of ethyl acetate. Chong et al. (2011), provided the CFD modeling for the photo catalytic oxidation of toluene and formaldehyde in a monolith reactor. In the reactor, the monoliths are considered as the porous medium and Langmuir – Hinshelwood (L–H) kinetics was used to model the photo catalytic oxidation on the monolith surfaces by fluent software. The results of the model showed that the reflectivity of the reactor wall had a significant effect on the reaction rate and overall conversion. Einaga et al. (2015), analyzed the behavior of photo catalytic ethylene oxidation in the fixed-bed reactors by CFD computations. The effect of gas flow rates and ethylene concentrations in the feed of rectangular and cylindrical reactors were evaluated. The k-ε turbulence model and L–H kinetics were selected to study the ethylene oxidation behavior in rectangular and cylindrical reactors at the different gas flow rates and ethylene concentrations in the inlet gas. Ansys-Fluent v. 12.1 commercial software was applied to prepare the acceptable model by using CFD. The results showed that the behavior of ethylene oxidation in the reactors depended heavily on the distribution of gas velocity and time of gas residence. During total catalytic toluene oxidation, Esparza-Isunza and López-Isunza developed a dynamic 2D two-phase model in a packed-bed catalytic reactor (Esparza-Isunza and López-Isunza, 2016). In the presented 2D model, the convection and axial and radial dispersions of heat and mass with Mars-van Krevelen's kinetic scheme were discretized using finite elements. The simulation achievements showed that the velocity of the gas stream and diameters of the reactor and catalyst particles were to be the significant parameters for a safe design. The photo catalytic oxidation of toluene was assessed by Nakahara et al. using CFD simulations (Nakahara et al., 2017). Ansys-Fluent v. 16.0 as the commercial CFD software was used with k–ε model, the Reynolds Averaged Navier–Stokes equation (RANS) and L–H kinetic mechanism. The results of the prediction of the exhaust concentration are reasonably consistent with those in experiments with a variance of less than 4%.

In spite of extensive studies in the explained research field, the challenge still remains to determine the performance of the supported catalysts for the simultaneous oxidation of VOCs in the binary mixture. Based on the open literature, the reaction kinetics studies have been one of the important pillars of the CFD modeling for a proper model. Therefore, the kinetic study requires the accurate solution of the partial differential equations derived from the governing equations which will be really time-consuming. Therefore, using artificial neural networks as a reliable method for kinetic modeling in the CFD studies will help to save time without solving any differential equations (Zabihi and Babajani, 2018).

The objective of the present work is to synthesize the supported cobalt oxide on the activated carbon by using the metal organic framework template for simultaneously removal of benzene and toluene from the polluted gas. The experimental results were also used to validate the CFD model. The hybrid modeling including neural network and CFD was then studied to illustrate the impact of temperature, initial pollutant concentration and reactor length. In particular, this study is aimed to:

- The experiment configuration was described.
- Multi-layer back-propagation neural network was applied to obtain a kinetic model for the catalytic reaction.
- Cylindrical oxidation reactor was simulated in COMSOL Multiphysics as a 2D physical model.
- The operating conditions and their effect on the total oxidation were investigated.
- The key parameters affecting the oxidation of benzene and toluene were studied.

2. Experimental

2.1. Preparation nano composite of supported cobalt oxide from Co-MOF@AC

The applied activated carbon in this study was prepared from the almond hard shell as described in our previous work (Zabihi et al., 2015), by physical activation method using water vapor. Initially, the solution of di-methyl formamide (DMF) and trimesic acid (H_3BTC) was prepared by using 50 mL of DMF and 0.5 g of H_3BTC for adding to the almond based activated carbon. The prepared solution was heated and mixed at 30 °C for 5 h. After that, the cobalt slat ($Co(NO_3)_2.6H_2O$) was added to the mixture of trimesic acid and the activated carbon, and the suspended solution was heated at 45 °C for 5 h on the stirrer. The generated solid was washed several times by mixture of deionized water and ethanol (1:1, V/V). The product was mixed by acetone and dried in the oven for 24 h. The dried nanocomposite was calcined at 200 °C under the nitrogen flow for 2 h while the heating rate was set at 10 °C/min. The fabricated cobalt based MOF was calcined at 500 °C under the nitrogen flow for about 2 h. Therefore, the supported cobalt oxide on the

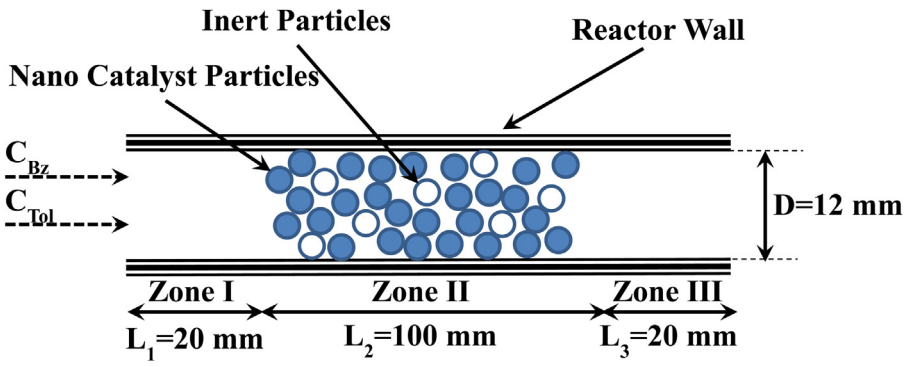

Fig. 1. Schematic of the catalytic reactor.

activated carbon was prepared as the final product derived from Co-MOF@AAC as the template.

The prepared nanocomposites of MOF and cobalt oxide were named Co-MOF@AAC and Co_3O_4@AAC (the used catalyst) for simplifying in the characterization tests and modeling, respectively. The used chemical materials were also purchased from Merck Company.

2.2. Characterization tests

Nitrogen adsorption/desorption to recognize the surface area and pore sizes were measured at 77 K using a BEL (Japan) and Brunauer–Emmett–Teller (BET) method. The X-ray diffraction (XRD) curve for the nano catalyst was plotted employing model D-64295 equipment from STOE Company. XRD test was accomplished at 30 kV, 20 mA, copper Ka radiation, and scanning rate of 3°/min. Morphologies of the prepared sample was evaluated using a field-emission scanning electron microscope (FESEM) by model TeScan-Mira III equipment from Czech Republic. The oxidation resistance of the supported cobalt oxide was studied by applying thermogravimetric analysis (TGA) utilizing a TGA-25 apparatus (Mettler-Toledo, Switzerland) by heating (rate of 10 °C $min^{-}1$) the 1 g of catalyst up to 1000 °C under the air flow of 55 cm^3 min^{-1} (STP).

2.3. Catalyst performance

The utilized experimental set-up was explained in our previous work with complete schematic (Zabihi et al., 2015). The tubular fixed reactor was applied for the investigation of deep oxidation of multiple feed with 200 mL/min flow rate including toluene and benzene over the Co_3O_4@AAC. The 1 g of fabricated catalyst was packed in the quartz reactor by using glass bead and wool with 100 and 12 mm in length and internal diameter, respectively. The temperature of reaction was evaluated by using PID controller in the center of the micro-reactor. The concentration of toluene, benzene, carbon dioxide and water vapor were measured online by using a gas chromatograph-mass spectroscopy (GC-Mass, Agilent, USA) system equipped with 5975C mass detector and a 30 m long HP-5MS stainless steel column. It must be pointed that there are no intermediate products such as carbon monoxide and hydrogen in this reactor which was described before (Zabihi et al., 2015). However, the conversion of species is calculated using the Eq. (1).

$$conversion\,\% = \frac{C_{A0} - C_A}{C_A} \times 100 \quad (1)$$

Where C_{A0} and C_A are input and output concentration of species, respectively.

3. Modeling procedure

The 2D physical configuration of cylindrical oxidation reactor illustrated schematically in Fig. 1 was simulated as the continuous porous medium in COMSOL Multiphysics (v.5.4). An unstructured tetrahedral mesh was exploited for the depicted domain in Fig. 1. The main advantageous of proposed model is the use of artificial neural network modeling rather than complex kinetics mechanisms. The intelligent modeling reduced the computational errors caused by complex mechanisms.

3.1. Governing equations

The fluid flow in the porous medium was affected by the solid particles which occupied the pore spaces (Zhuang et al., 2012). The following assumptions were considered for the writing of the governing equations after the geometry was specified.

- The bulk fluid viscosity and density were to be constant in entire micro-reactor (At operating temperature and average pressure inside the micro-reactor).
- The porosity of micro-reactor was considered to be constant.
- The diffusion mass transfer coefficient for all components in the entire micro-reactor was assumed to be constant; and
- The operating conditions were stayed constant as time passes.

The continuity and momentum balance equations of the Navier Stokes based on the pointed assumptions along with the other main governing and supplementary equations in matrix form are listed in Table 1.

3.2. Boundary conditions

Between the polluted air and the micro-reactor wall, the non-slip boundary condition was brought up for the calculation of the fluid velocity. The operating conditions of the feed including C_0 = 1000 ppmv, and Q_0 = 200 mL/min were applied at the inlet of micro-reactor. In addition, the temperature, the pressure and the porosity were considered to be about 20 °C, 1 atm and 30 %, respectively.

3.3. Algorithm of neural network and CFD

To model the kinetic behavior of the catalytic oxidation, artificial neural network was designed by using a three-layer back-propagation network consisting of the input, hidden and output layers as shown in Fig. 2. The Oxidation temperature (A), the initial concentration of benzene (B) and toluene (C) were variables of input layer in designed network. The specific weights were multiplied input data and added to the threshold values. The calculated

Table 1
The used governing and supplementary equations.

Zone I & III	Continuity Equation	$\rho(u.\nabla)u = \nabla.[-pI + K]$; $K=\mu(\nabla u + (\nabla u)^T)$; $\rho\nabla.(u) = 0$;
	Fick's Laws of Diffusion	$\nabla.J_i + u.\nabla C_i = 0$; $J_i=-D_i\nabla C_i$;
	Continuity Equation	$\frac{1}{C_p}\rho(u.\nabla)u\frac{1}{C_p} = \nabla.[-pI + K] - (\mu\kappa^{-1}+b_F)u$; $\rho\nabla.(u) = 0$;
		$K=\mu\frac{1}{C_p}(\nabla u + (\nabla u)^T) - \frac{2}{3}\mu\frac{1}{C_p}(\nabla.u)I$
Zone II	Forchheimer Coefficient	$b_F = \frac{C_f \cdot C_p \cdot \rho}{\sqrt{\kappa}}$;
	Friction Coefficient	$C_f = \frac{1.75}{\sqrt{150\varepsilon_p^3}}$;
	Permeability: Kozeeny Carman	$\kappa = \frac{d_p^2\varepsilon_p^3}{180*(1-\varepsilon_p)^2}$
	Fick's laws of diffusion	$\nabla.J_i + u.\nabla C_i = R_i$; $J_i=-D_{e,i}\nabla C_i$;
	Tortuosity: Millington and Quirk Model	$D_{e,i} = \frac{\varepsilon_p}{\tau_i}D_i$; $\tau_i = \varepsilon_p^{-1/3}$;

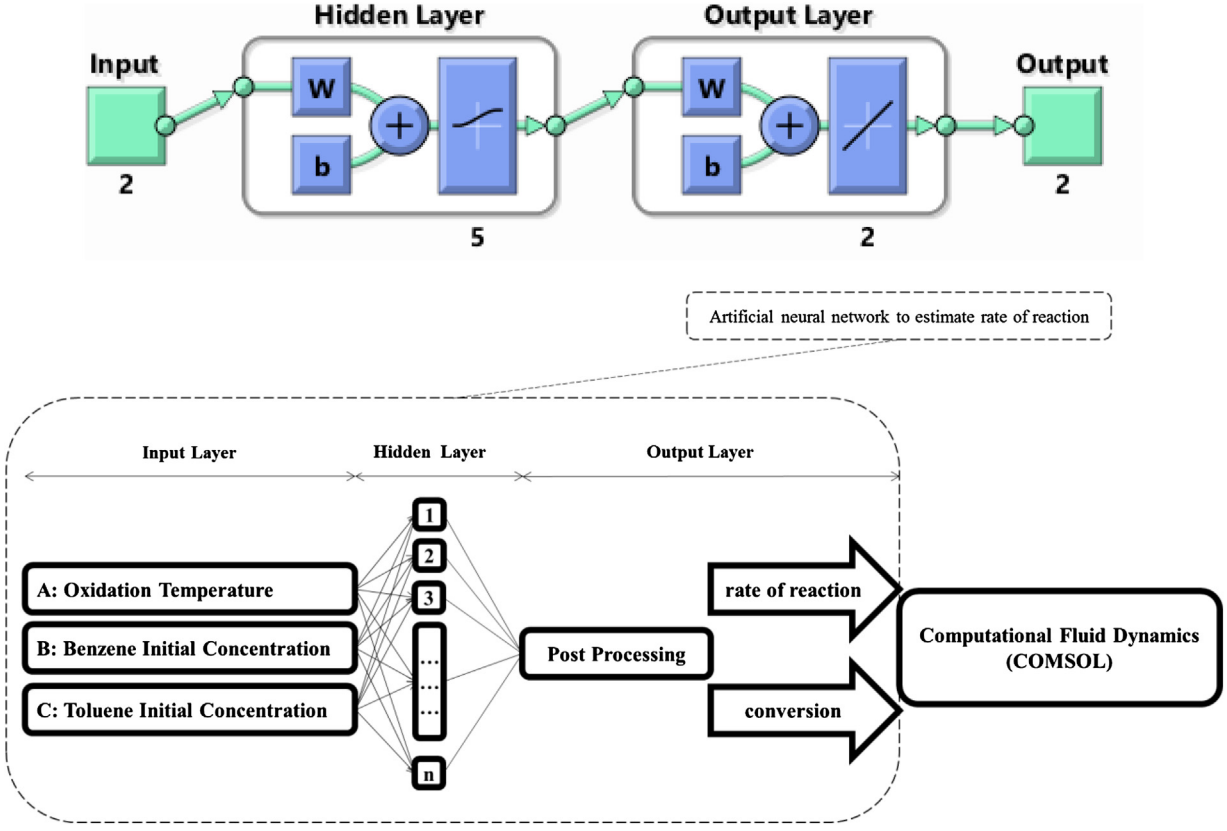

Fig. 2. Architecture of the used CFD-ANN hybrid modeling.

results were then used as the feeds in the hidden layer for each neuron. The transfer function was determined "logsig" and "purelin" for the hidden and output layer, respectively.

The training function named "trainlm" was employed to update the weights and thresholds. To find the optimal size of the back-propagation network, the training algorithm was studied with different number of neurons from 1 to 20. In the present work, 20 data points were collected from experimental runs to construct the proposed network. The experimental data was divided to three groups including validation (20 %), test (20 %) and training (60 %). It must be noted that the neural network modeling was coded by applying Matlab V. 2018b software.

Defined as Eqs (2) and (3) similar to (Zabihi and Babajani, 2018), and (Abdoli et al., 2018), the determination coefficient (R^2) and the mean square errors (MSE) were estimated from the calculation of 100 epochs for each training algorithm.

$$R^2 = \frac{\sum_{i=1}^{n}(x_{i,exp} - x_{avg})^2 - \sum_{i=1}^{n}(x_{i,exp} - x_{i,cfd})^2}{\sum_{i=1}^{n}(x_{i,exp} - x_{avg})^2} \quad (2)$$

$$MSE = \frac{1}{n}\sum_{i=1}^{n}(x_{i,exp} - x_{i,cfd})^2 \quad (3)$$

Where $x_{i,exp}$, x_{avg}, and $x_{i,cfd}$ are the experimental, average of experimental and the results of CFD modeling conversion, respectively.

It must be mentioned that he experimental data was obtained in two set including constant reaction temperature and constant initial concentration of VOCs. The neural network modeling was applied for the calculation of reaction rate as explained before. Therefore, the exit concentration of VOCs at the end of reactor was achieved by employing the summarized equations in Table 1 and the calculated rate of reaction in COMSOL software. Then, the conversion of VOCs in the simultaneous deep combustion was measured with knowing the initial and exit concentration of VOCs by Eq. 1. The explained method was added to the revised manuscript.

The summarized equations in Table 1 were solved by COMSOL Multiphysics. The governing equations are discretized by the finite element method (FEM) in a non-uniform structural mesh. Analysis of grid independence was carried out to achieve the most suitable mesh number (86,086 domain elements and 2346 boundary elements) for the physical model and a non-uniform mesh of was lastly chosen. The technique of sub-relaxation iteration was used for CFD simulations to guarantee convergence of simulations. Furthermore, the simulation runs were carried out in a 3.20 GHz Core i7 CPU with 32 GB of RAM.

4. Results and discussion

4.1. Catalyst characterizations

The XRD patterns of Co-MOF@AAC and Co_3O_4@AAC were studied and compared with the similar metal organic framework presented in the previous work (Punde et al., 2018) in Fig. 3. The weak and sharp peaks at 2θ = 17.5°, 18.70°, and 27.15° were related to the formation of cobalt based MOF in the presence of the activated carbon according to the pointed study (Punde et al., 2018). The amorphous phase is corresponded to the almond based activated carbon (Zabihi and Babajani, 2018). The low intensity of detected peaks indicated the high dispersion of $Co_3(BTC)_2$ crystallites over the porous activated carbon as seen in Fig. 3a.

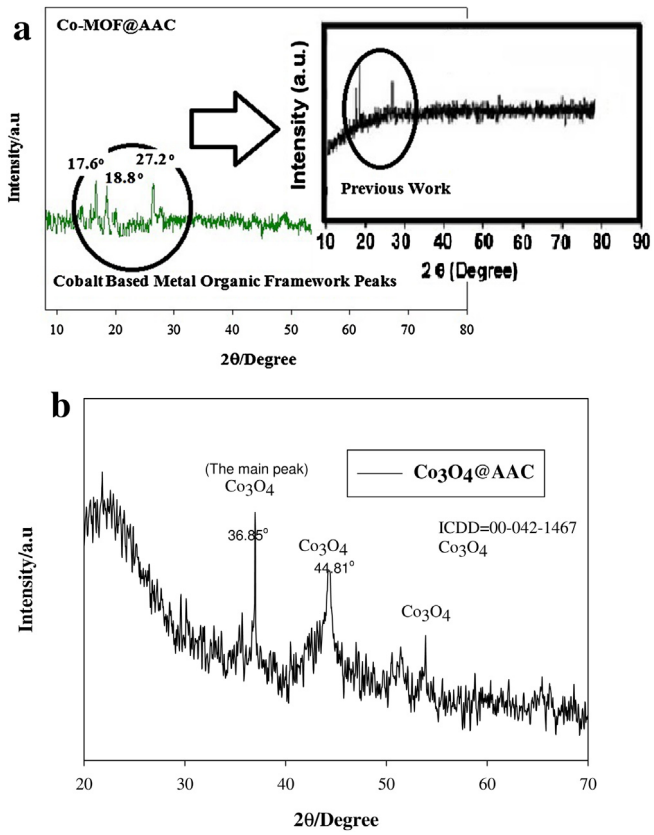

Fig. 3. a. XRD pattern of Co-MOF@AAC sample. b. XRD pattern of Co_3O_4@AAC sample.

Fig. 3b also shows the XRD pattern of Co_3O_4@AAC which was studied by Xpert-HighScore software (v.1) and ICDD codes. The Co_3O_4 crystallites were also detected according to ICDD = 00-042-1467 which illustrated that the formed peak at 2θ = 36.85° was related to the formation of cobalt oxide on the activated carbon.

The size of detected crystallite was estimated to be below of 40 nm by using Scherrer equation (Didehban et al., 2018; Soltani and Zabihi, 2020).

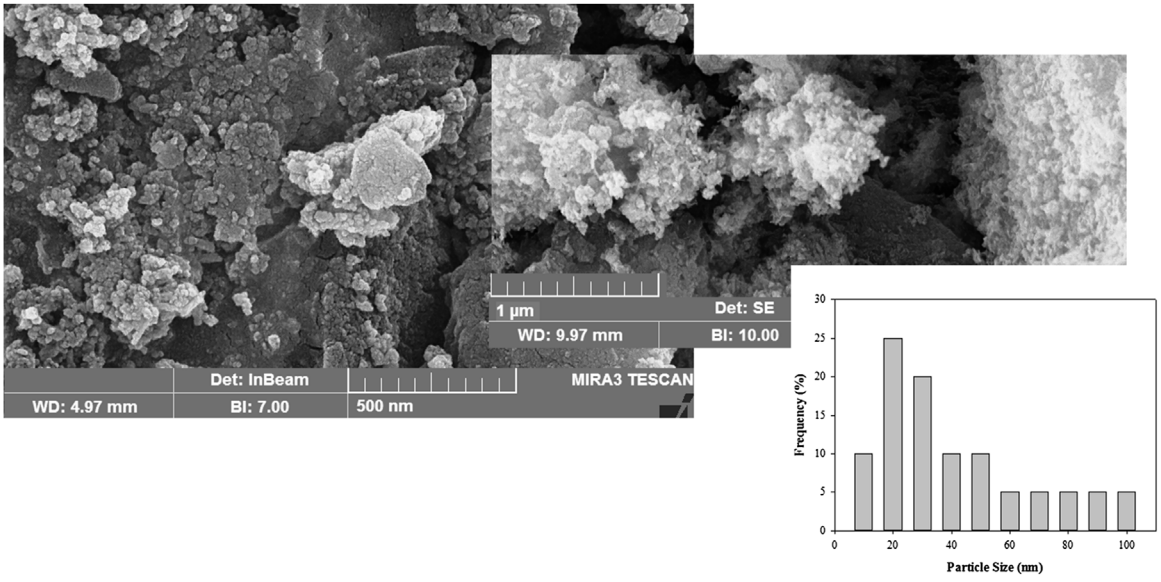

Fig. 4. FESEM results of Co_3O_4@AAC sample.

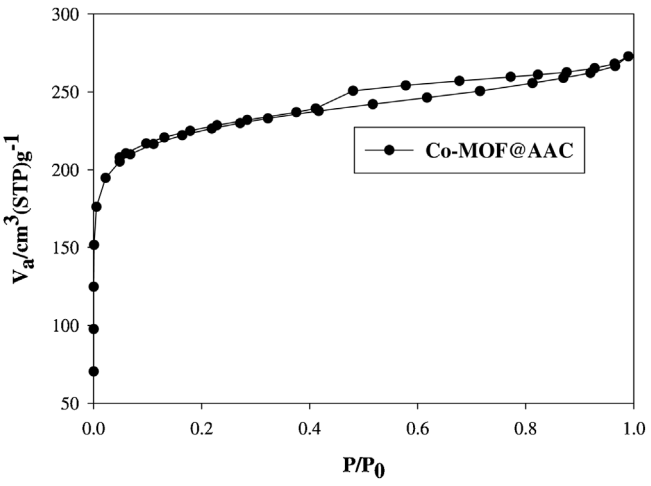

Fig. 5. Nitrogen adsorption-desorption of Co_3O_4@AAC sample.

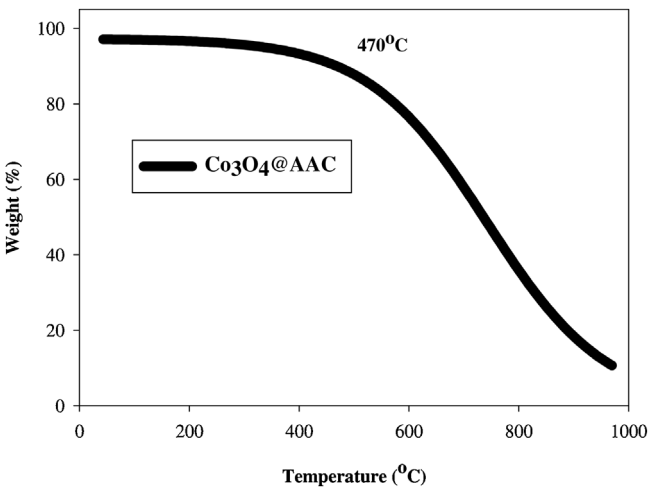

Fig. 6. TGA analysis of Co_3O_4@AAC sample.

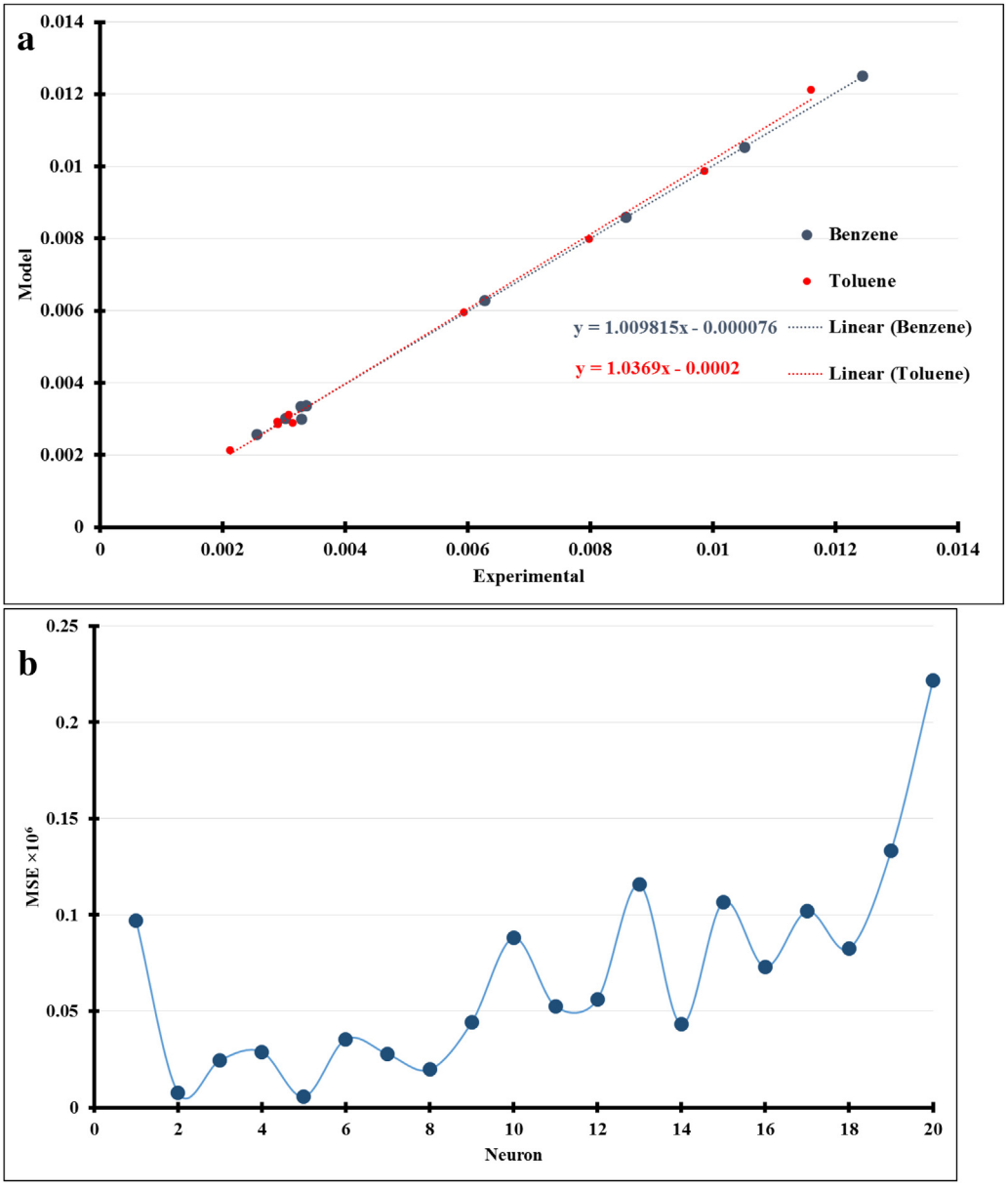

Fig. 7. a. Plotted ANN output versus experimental data. b. Effect of neuron number on the MSE.

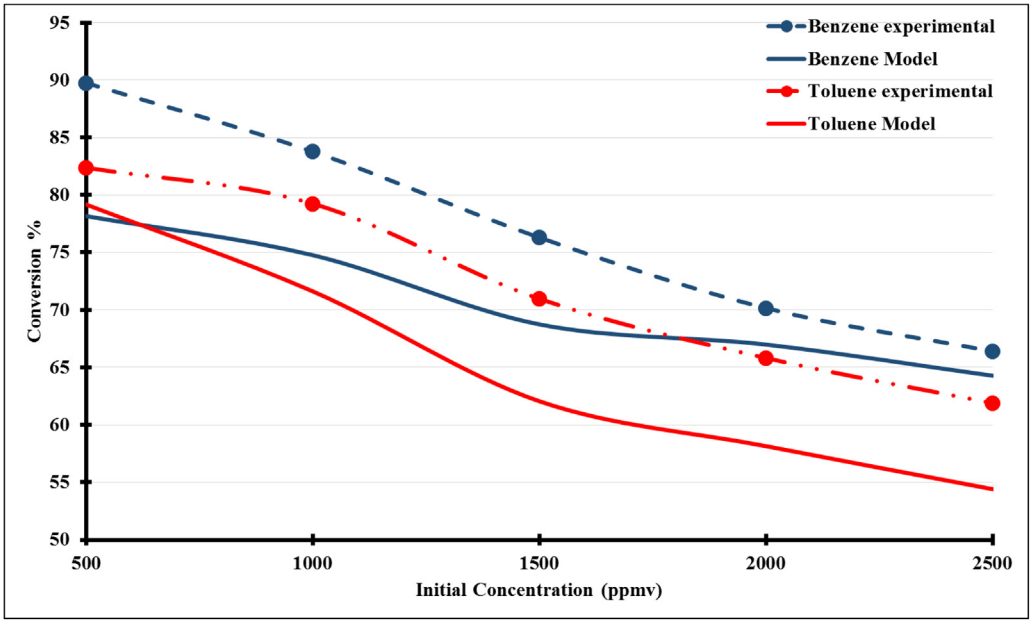

Fig. 8. Conversion vs. initial concentration for benzene and toluene (T = 250 °C, Q_0 = 200 mL/min and catalyst dosage = 1 g).

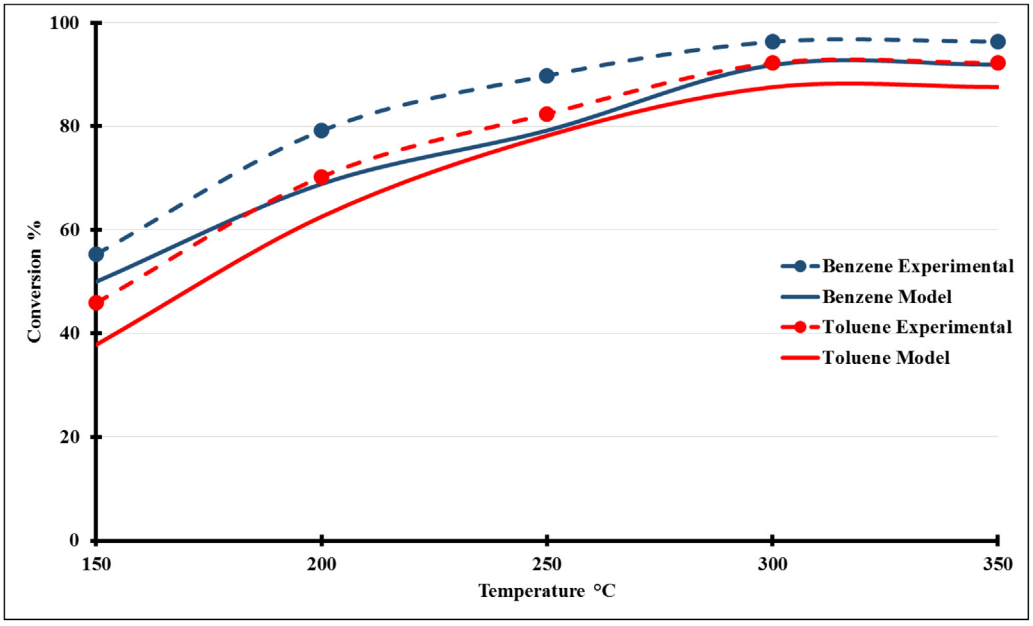

Fig. 9. Conversion vs. temperature for benzene and toluene (C_0 = 500 ppm, Q_0 = 200 mL/min and catalyst dosage = 1 g).

The morphology of prepared nanocomposite was characterized by using FESEM analysis as seen in Fig. 4. The well dispersed supported cobalt oxide was observed on the mesoporous activated carbon with the spherical shape. The size of nanoparticles was measured by using Clemex software and the frequency distribution was plotted in Fig. 4. As obtained results, the FESEM micro-images can be in the appropriate agreement with the XRD and Scherrer achievements. The results demonstrated that the supported cobalt oxide nanoparticles were fabricated in size below of 40 nm.

The nitrogen adsorption-desorption on the synthesized MOF catalysts was conducted to determine the surface area and total pore volume of sample by using BET model. As depicted hysteresis curve in Fig. 5, the prepared sample was produced with mesoporous structure which was confirmed by IUPAC classification (IV type). According to our previous work (Zabihi et al., 2015), the almond based activated carbon with the mesoporous structure was derived by physical activation. Therefore, the preparation method and the formation of cobalt - MOF had no significant effect on the structure of prepared activated carbon. The surface area and total pore volume of almond based activated carbon were calculated to be 860.70 m^2/g and 0.4697 cm^3/g, respectively. In the present study, the surface area and total pore of Co_3O_4@AAC were also measured to be 690 m^2/g and 0.3762 cm^3/g, respectively which were in the good agreement with the reported results in the similar previous work (Fleker et al., 2016).

One of the significant properties of the applied catalysts in the oxidation of VOCs is the resistance to the oxidation which can be analyzed by TGA test as seen in Fig. 6. The results clearly show that no weight loss and burning off of the synthesized catalyst occur at the temperatures below 470 °C. It must be pointed that the

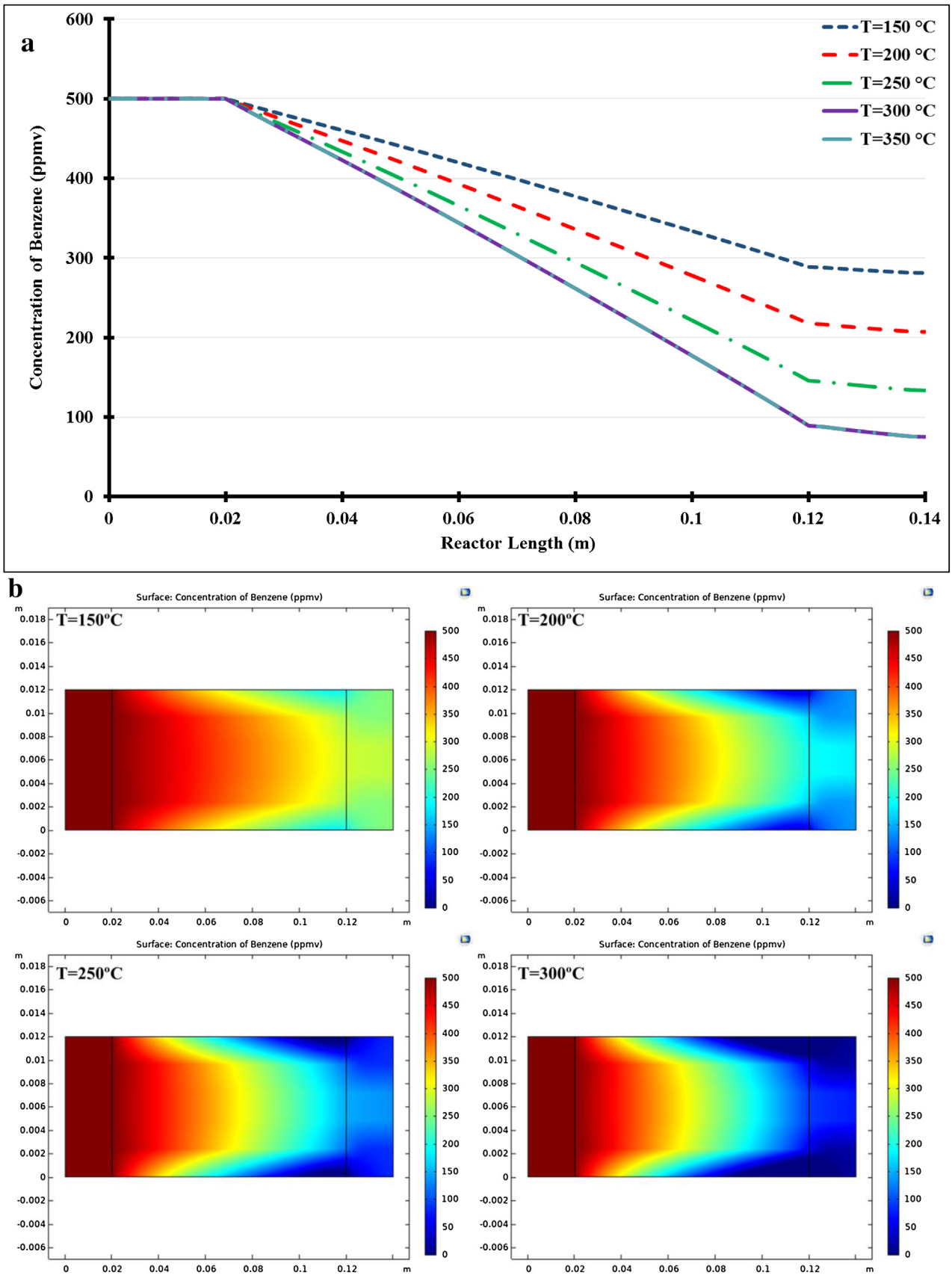

Fig. 10. a. The variations of benzene concentration along the reactor. b. The benzene concentration contours in the micro-reactor.

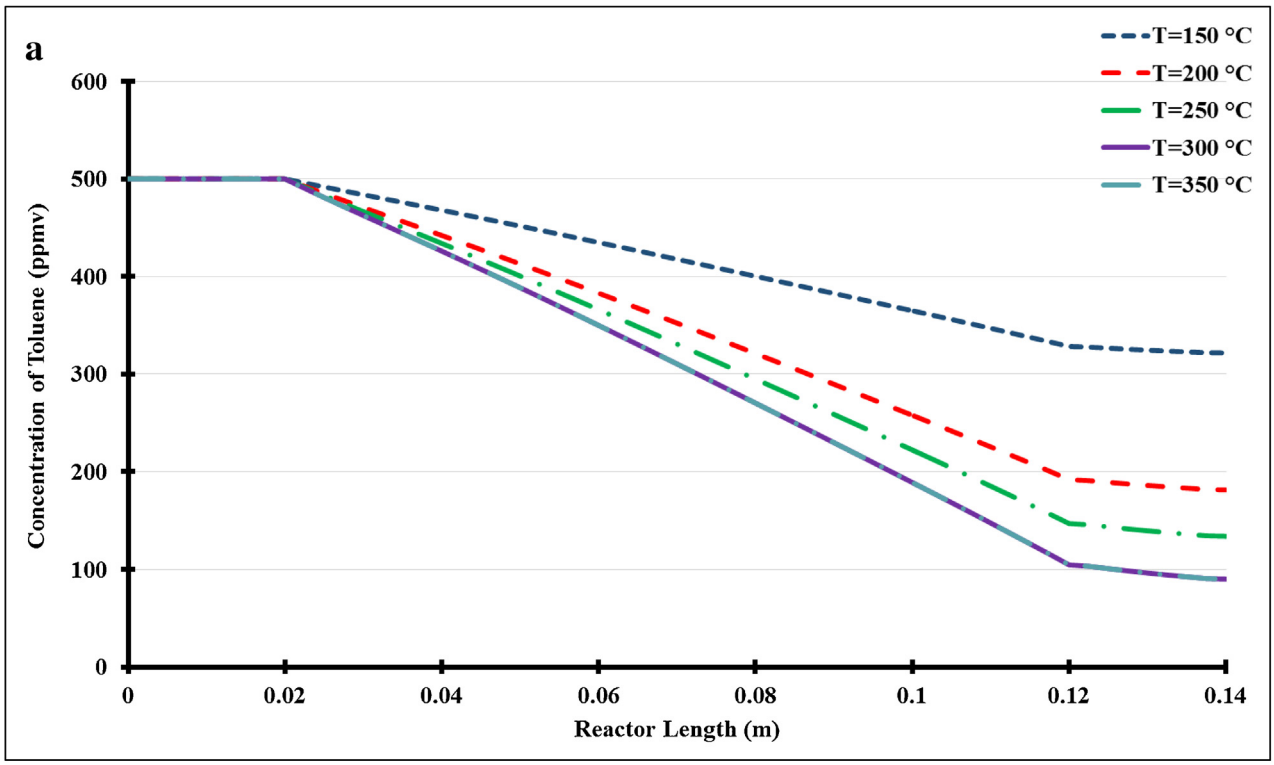

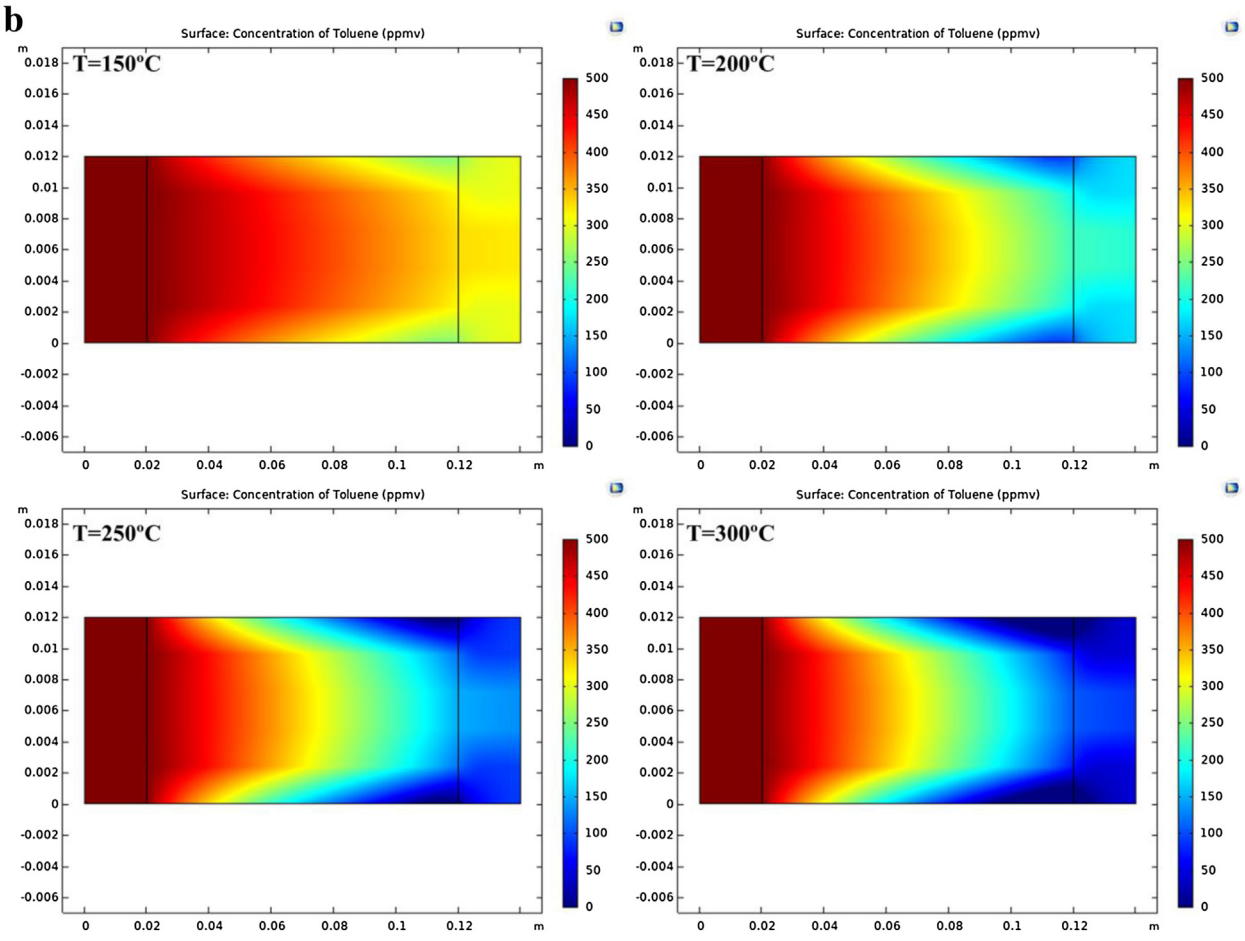

Fig. 11. a. The variations of toluene concentration along the reactor. b. The toluene concentration contours in the micro-reactor.

almond hard shell based activated carbon was carbonized at 800 °C as explained in the previous work (Zabihi et al., 2015) and the heating process of cobalt oxide catalyst was carried out at 500 °C. The results also determined that the reduction of catalyst weight was observed with increasing the temperature from 470 to 960 °C. Therefore, the cobalt oxide catalyst supported on the activated carbon (Co_3O_4@AAC) can be the proper sample for the complete combustion of VOCs.

4.2. Model validation

Fig. 7 indicated the results of MSE and correlation coefficient values versus the number of neurons in the hidden layer to achieve the proper network for the kinetic study. The minimum MSE and maximum correlation coefficient were calculated to be about 5 and 0.99, respectively which illustrated that there is an appropriate consistent between the experimental data and the neural network modeling. Therefore, the numerical modeling can be substituted instead of theoretical model to investigate the kinetic behavior of the catalytic oxidation.

In order to validate the CFD simulation incorporated with neural network modeling, domain size and boundary conditions were the same as those used in experiments and the simulation results were compared with the experimental observations. Fig. 8 demonstrates the comparison between the modeling achievements and experimental data for the deep simultaneous conversion of benzene and toluene at the various initial concentrations in the range of 500–2500 ppmv (initial concentration ratio: 50:50 V/V %) while the other operating conditions kept constant.

The offered results in Fig. 8 indicate that the maximum conversion of VOCs was measured at 500 ppmv and the total conversion decreased with increasing the initial concentrations similar to the previous works (He et al., 2010; Zabihi et al., 2015). The important reason for the reduction of catalyst activity can be descripted by forming the by-products including water vapor and carbon dioxide over the surface of the prepared sample. Based on the experimental results, the maximum conversion of benzene and toluene were calculated to be 89.74 % and 82.37 %, respectively. As can be seen from Fig. 8, the modeling results are in good agreement with the experimental data according to the obtained results including R^2 = 0.92, MSE = 0.05.

Fig. 9 also illustrates the total conversion of benzene and toluene during complete oxidation in air over the synthesized catalyst. Experiments were conducted over 1 g of catalyst at the different reaction temperatures (150−350 °C) while the concentration of VOCs was to be 500 ppmv in the feed. As shown in Fig. 9, the conversion of toluene and benzene boosted by increasing the oxidation temperature in the binary solutions. The conversion of VOCs increased sharply in the initial stages (150−300 °C) when the mildly increasing was detected at the temperatures upper than 300 °C for both benzene and toluene. In continued, the results showed that the performance of the prepared catalyst was higher for benzene compared with toluene which can be justified by the adsorption strength and the chemical structure of toluene and benzene. The similar results were also reported in the open literature (He et al., 2010). The computational modeling also was evaluated for the effect of oxidation temperature as seen in Fig. 9, which illustrated the appropriate consistent with the experimental results as calculated correlation coefficient and mean square error (R^2 = 0.92 and MSE = 0.03). Finally, the model is capable of exploring certain variables of impact on the VOCs catalytic oxidation.

4.3. Evaluation of VOCs concentration in along the reactor

The obtained calculations showed that there is a good agreement between the numerical model and experimental data. Therefore, the model was applied to display the concentration of benzene and toluene along the reactor at the various oxidation temperatures. Fig. 10a shows the variation of benzene concentration in the reactor while the reaction temperature increased from 150 to 350 °C. The obtained results demonstrated that the concentration of benzene reduced linearly in the reactor and the difference between the concentration of benzene at the high temperatures (300 and 350 °C) can be ignored along the reactor. In the other word, the simultaneous conversion of benzene was enhanced linearly along the reactor. The contour of benzene concentration was also plotted in Fig. 10b, which confirms the mentioned results obtained from Fig. 10a. The conversion of benzene gradually decreased considering plug flow without axial dispersion. The similar behavior was studied for the toluene oxidation in the presence of benzene in air as shown in Fig. 11. However, the increase of temperature on the catalyst performance for the oxidation of toluene at the low temperature was remarkable effect. The higher conversion near the wall was achieved due to the higher retention time near the wall as indicated in the contours.

5. Conclusion

A hybrid modeling using CFD and ANN was applied to design an intelligent model to study the simultaneous catalytic oxidation of benzene and toluene in the porous micro-reactor. Nano-supported cobalt oxide on the almond based activated carbon was prepared by using the metal organic framework as a template in the presence of trimesic acid. Maximum conversion of benzene and toluene were obtained to be about 89.74 % and 82.37 % at 350 °C, respectively. The catalytic activity of the synthesized sample was found to be enhanced with increasing and reducing the oxidation temperature and initial concentration of VOCs, respectively. It is very complex to derive the kinetic mechanism for the simultaneous deep conversion of VOCs over the catalyst in the dynamics fluid studies. Therefore, the kinetic rates were measured by using ANN modeling to avoid the solving the partial differential equations. The calculated correlation coefficient (0.99) of the ANN model with 5 neurons and logsig as a transfer function of the hidden layer illustrated the successful modeling to measure the reaction rates. The results of established CFD model were also in the good agreement with the experimental data while the value of R^2 was to be o.92. The achievements of contours also illustrated that the concentration of VOCs decreases along the reaction linearly. Finally, the recommended model can be employed for the complex simultaneous oxidation of VOCs in the plug reactor without involving in the kinetic mechanism.

Declaration of Competing Interest

There is no financial interests/personal relationships in this work.

Acknowledgements

The authors are greatly acknowledging the assistance of environmental engineering research center, Sahand University of Technology, Tabriz, Iran. We would like to show our gratitude to Biofluid laboratory in Sahand University of Technology for supporting the computational equipments in this project.

References

Abdoli, S.M., Shafiei, S., Raoof, A., Ebadi, A., Jafarzadeh, Y., Aslannejad, H., 2018. Water flux reduction in microfiltration membranes: a pore network study. Chem. Eng. Technol. 41, 1566–1576, http://dx.doi.org/10.1002/ceat.201800130.

Anjum, H., Johari, K., Gnanasundaram, N., Appusamy, A., Thanabalan, M., 2019. Impact of surface modification on adsorptive removal of BTX onto activated

carbon. J. Mol. Liq. 280, 238–251, http://dx.doi.org/10.1016/j.molliq.2019.02.046.
Azalim, S., Brahmi, R., Bensitel, M., Giraudon, J.-M., Lamonier, J.-F., 2010. Preparation and characterization of nanocrystallines Mn-Ce-Zr mixed oxide catalysts by sol-gel method: application to the complete oxidation of n-butanol. Stud. Surf. Sci. Catal., 731–734, http://dx.doi.org/10.1016/S0167-2991(10)75147-8.
Bandura, L., Kołodyńska, D., Franus, W., 2017. Adsorption of BTX from aqueous solutions by Na-P1 zeolite obtained from fly ash. Process Saf. Environ. Prot. 109, 214–223, http://dx.doi.org/10.1016/j.psep.2017.03.036.
Binas, V., Stefanopoulos, V., Kiriakidis, G., Papagiannakopoulos, P., 2019. Photocatalytic oxidation of gaseous benzene, toluene and xylene under UV and visible irradiation over Mn-doped TiO2 nanoparticles. J. Mater. 5, 56–65, http://dx.doi.org/10.1016/j.jmat.2018.12.003.
Bounaceur, R., Da Costa, I., Fournet, R., Billaud, F., Battin-Leclerc, F., 2005. Experimental and modeling study of the oxidation of toluene. Int. J. Chem. Kinet. 37, 25–49, http://dx.doi.org/10.1002/kin.20047.
Chen, Z., Wang, Y., Liang, Q., Chen, L., Zhan, W., Li, Y., 2020. Structure-induced hollow Co3O4 nanoparticles with rich oxygen vacancies for efficient CO oxidation. Sci. China Mater. 63, 267–275, http://dx.doi.org/10.1007/s40843-019-1178-5.
Chong, S., Wang, S., Tade, M., Ang, H.M., Pareek, V., 2011. Simulations of photodegradation of toluene and formaldehyde in a monolith reactor using computational fluid dynamics. AICHE J. 57, 724–734.
Choya, A., de Rivas, B., González-Velasco, J.R., Gutiérrez-Ortiz, J.I., López-Fonseca, R., 2020. Oxidation of lean methane over cobalt catalysts supported on ceria/alumina. Appl. Catal. A Gen. 591, 117381, http://dx.doi.org/10.1016/j.apcata.2019.117381.
Da Costa, I., Fournet, R., Billaud, F., Battin-Leclerc, F., 2003. Experimental and modeling study of the oxidation of benzene. Int. J. Chem. Kinet. 35, 503–524, http://dx.doi.org/10.1002/kin.10148.
Deng, H., Kang, S., Wang, C., He, H., Zhang, C., 2018. Palladium supported on low-surface-area fiber-based materials for catalytic oxidation of volatile organic compounds. Chem. Eng. J. 348, 361–369, http://dx.doi.org/10.1016/j.cej.2018.04.184.
Derco, J., Šimovičová, K., Dudáš, J., Valičková, M., 2017. Removal of BTX contaminants with O3 and O3/UV processes, in: physico-chemical wastewater treatment and resource recovery. InTech., http://dx.doi.org/10.5772/65889.
Didehban, A., Zabihi, M., Shahrouzi, J.R., 2018. Experimental studies on the catalytic behavior of alloy and core-shell supported Co-Ni bimetallic nano-catalysts for hydrogen generation by hydrolysis of sodium borohydride. Int. J. Hydrogen Energy 43, 20645–20660, http://dx.doi.org/10.1016/j.ijhydene.2018.09.127.
Einaga, H., Tokura, J., Teraoka, Y., Ito, K., 2015. Kinetic analysis of TiO2-catalyzed heterogeneous photocatalytic oxidation of ethylene using computational fluid dynamics. Chem. Eng. J. 263, 325–335, http://dx.doi.org/10.1016/j.cej.2014.11.017.
Esparza-Isunza, T., López-Isunza, F., 2016. Modeling the transient VOC (toluene) oxidation in a packed-bed catalytic reactor. Int. J. Chem. React. Eng. 14, 1177–1185, http://dx.doi.org/10.1515/ijcre-2016-0026.
Fiorenza, R., Crisafulli, C., Condorelli, G.G., Lupo, F., Scirè, S., 2015. Au–Ag/CeO2 and Au–Cu/CeO2 catalysts for volatile organic compounds oxidation and CO preferential oxidation. Catal. Letters 145, 1691–1702, http://dx.doi.org/10.1007/s10562-015-1585-5.
Fleker, O., Borenstein, A., Lavi, R., Benisvy, L., Ruthstein, S., Aurbach, D., 2016. Preparation and properties of metal organic Framework/Activated carbon composite materials. Langmuir 32, 4935–4944, http://dx.doi.org/10.1021/acs.langmuir.6b00528.
He, C., Li, P., Cheng, J., Hao, Z.P., Xu, Z.P., 2010. A comprehensive study of deep catalytic oxidation of benzene, toluene, ethyl acetate, and their mixtures over Pd/ZSM-5 catalyst: mutual effects and kinetics. Water Air Soil Pollut. 209, 365–376, http://dx.doi.org/10.1007/s11270-009-0205-7.
Hyodo, T., Hashimoto, T., Ueda, T., Nakagoe, O., Kamada, K., Sasahara, T., Tanabe, S., Shimizu, Y., 2015. Adsorption/combustion-type VOC sensors employing mesoporous γ-alumina co-loaded with noble-metal and oxide. Sens. Actuators B Chem. 220, 1091–1104, http://dx.doi.org/10.1016/j.snb.2015.06.065.
Jafari, A.J., Kalantary, R.R., Esrafili, A., Arfaeinia, H., 2018. Synthesis of silica-functionalized graphene oxide/ZnO coated on fiberglass and its application in photocatalytic removal of gaseous benzene. Process Saf. Environ. Prot. 116, 377–387, http://dx.doi.org/10.1016/j.psep.2018.03.015.
Jeon, M.-J., Jeon, Y.-W., 2017. Characteristic evaluation of activated carbon applied to a pilot-scale VSA system to control VOCs. Process Saf. Environ. Prot. 112, 327–334, http://dx.doi.org/10.1016/j.psep.2017.05.009.
Lee, S.M., Hwang, I.-H., Lee, D.Y., Kim, S.S., 2020. A new combined electrolysis and catalytic system for removal of VOCs. Chem. Eng. J. 382, 123032, http://dx.doi.org/10.1016/j.cej.2019.123032.
Li, C., Zhang, F., Feng, S., Wu, H., Zhong, Z., Xing, W., 2018. SiC@TiO 2 /Pt catalytic membrane for collaborative removal of VOCs and nanoparticles. Ind. Eng. Chem. Res. 57, 10564–10571, http://dx.doi.org/10.1021/acs.iecr.8b02264.
Li, J.-R., Wang, F.-K., He, C., Huang, C., Xiao, H., 2020a. Catalytic total oxidation of toluene over carbon-supported Cu Co oxide catalysts derived from Cu-based metal organic framework. Powder Technol. 363, 95–106, http://dx.doi.org/10.1016/j.powtec.2019.12.060.
Li, J.R., Wang, F.K., He, C., Huang, C., Xiao, H., 2020b. Catalytic total oxidation of toluene over carbon-supported Cu[sbnd]Co oxide catalysts derived from Cu-based metal organic framework. Powder Technol. 363, 95–106, http://dx.doi.org/10.1016/j.powtec.2019.12.060.
Liang, P., Jiang, W., Zhang, L., Wu, J., Zhang, J., Yang, D., 2015. Experimental studies of removing typical VOCs by dielectric barrier discharge reactor of different sizes. Process Saf. Environ. Prot. 94, 380–384, http://dx.doi.org/10.1016/j.psep.2014.09.003.
Liu, X., Wang, J., Zeng, J., Wang, X., Zhu, T., 2015. Catalytic oxidation of toluene over a porous Co3O4-supported ruthenium catalyst. RSC Adv. 5, 52066–52071, http://dx.doi.org/10.1039/c5ra07072d.
Łojewska, J., Kołodziej, A., Łojewski, T., Kapica, R., Tyczkowski, J., 2009. Structured cobalt oxide catalyst for VOC combustion. Part I: catalytic and engineering correlations. Appl. Catal. A Gen. 366, 206–211, http://dx.doi.org/10.1016/j.apcata.2009.07.006.
Lopes, R.J.G., Silva, A.M.T., Quinta-Ferreira, R.M., 2007. Kinetic modeling and trickle-bed CFD studies in the catalytic wet oxidation of vanillic acid. Ind. Eng. Chem. Res. 46, 8380–8387, http://dx.doi.org/10.1021/ie070009a.
Lu, Y., Li, Y., Liu, D., Ning, Y., Yang, S., Yang, Z., 2020. Adsorption of benzene vapor on natural silicate clay minerals under different moisture contents and binary mineral mixtures. Colloids Surf. A Physicochem. Eng. Asp. 585, 124072, http://dx.doi.org/10.1016/j.colsurfa.2019.124072.
Luo, Y., Zheng, Y., Zuo, J., Feng, X., Wang, X., Zhang, T., Zhang, K., Jiang, L., 2018. Insights into the high performance of Mn-Co oxides derived from metal-organic frameworks for total toluene oxidation. J. Hazard. Mater. 349, 119–127, http://dx.doi.org/10.1016/j.jhazmat.2018.01.053.
Montero-Montoya, R., López-Vargas, R., Arellano-Aguilar, O., 2018. Volatile organic compounds in air: sources, distribution, exposure and associated illnesses in children. Ann. Glob. Heal. 84, 225–238, http://dx.doi.org/10.29024/aogh.910.
Nakahara, K., Yamaguchi, T., Lim, E., Ito, K., 2017. Computational fluid dynamics modeling and parameterization of the visible light photocatalytic oxidation process of toluene for indoor building material. Sustain. Cities Soc. 35, 298–308, http://dx.doi.org/10.1016/j.scs.2017.08.020.
Niaei, A., Salari, D., Hosseini, S.A., Nabavi, R., Jodaei, A., 2008. CFD simulation of catalytic oxidation of ethyl acetate over Cr-HZSM-5 catalyst. Int. J. Chem. React. Eng., 6.
Nowicka, E., Sankar, M., 2018. Designing Pd-based supported bimetallic catalysts for environmental applications. J. Zhejiang Univ. A 19, 5–20, http://dx.doi.org/10.1631/jzus.A1700257.
Pham, T.H., Than, H.A.Q., Bui, H.M., 2019. The catalytic oxidation of toluene at low temperature over palladium nanoparticles supported on Alumina sphere catalysts: effects of Palladium precursors and preparation method. Polish J. Chem. Technol. 21, 48–50, http://dx.doi.org/10.2478/pjct-2019-0038.
Popova, M., Boycheva, S., Lazarova, H., Zgureva, D., Lázár, K., Szegedi, Á., 2019. VOC oxidation and CO2 adsorption on dual adsorption/catalytic system based on fly ash zeolites. Catal. Today, 1–8, http://dx.doi.org/10.1016/j.cattod.2019.06.070.
Punde, N.S., Rawool, C.R., Rajpurohit, A.S., Karna, S.P., Srivastava, A.K., 2018. Hybrid composite based on porous cobalt-benzenetricarboxylic acid metal organic framework and graphene nanosheets as high performance supercapacitor electrode. ChemistrySelect 3, 11368–11380, http://dx.doi.org/10.1002/slct.201802721.
Rajamanickam, R., Baskaran, D., Kaliyamoorthi, K., Baskaran, V., Krishnan, J., 2020. Steady State, transient behavior and kinetic modeling of benzene removal in an aerobic biofilter. J. Environ. Chem. Eng. 8, 103657, http://dx.doi.org/10.1016/j.jece.2020.103657.
Russo, A.V., Andrade, C.V., De Angelis, L.E., Jacobo, S.E., 2018. Adsorption and catalytic oxidation of organic pollutants using Fe-zeolite. Water Sci. Technol. 77, 939–947, http://dx.doi.org/10.2166/wst.2017.611.
Sedjame, H.J., Fontaine, C., Lafaye, G., Barbier, J., 2014. On the promoting effect of the addition of ceria to platinum based alumina catalysts for VOCs oxidation. Appl. Catal. B Environ. 144, 233–242, http://dx.doi.org/10.1016/j.apcatb.2013.07.022.
Soltani, M., Zabihi, M., 2020. Hydrogen generation by catalytic hydrolysis of sodium borohydride using the nano-bimetallic catalysts supported on the core-shell magnetic nanocomposite of activated carbon. Int. J. Hydrogen Energy, http://dx.doi.org/10.1016/j.ijhydene.2020.02.203.
Tabakova, T., Ilieva, L., Petrova, P., Venezia, A.M., Avdeev, G., Zanella, R., Karakirova, Y., 2015. Complete benzene oxidation over mono and bimetallic Au–Pd catalysts supported on Fe-modified ceria. Chem. Eng. J. 260, 133–141, http://dx.doi.org/10.1016/j.cej.2014.08.099.
Tidahy, H.L., Siffert, S., Lamonier, J.-F., Zhilinskaya, E.A., Aboukaïs, A., Yuan, Z.Y., Vantomme, A., Su, B.-L., Canet, X., Deweireld, G., Frère, M., 2007a. Characterisation of new Pd / hierarchical macro-mesoporous ZrO2, TiO2 and ZrO2-TiO2 catalysts for toluene total oxidation. Stud. Surf. Sci. Catal., 201–208, http://dx.doi.org/10.1016/S0167-2991(07)80027-9.
Tidahy, H.L., Siffert, S., Lamonier, J.F., Cousin, R., Zhilinskaya, E.A., Aboukaïs, A., Su, B.L., Canet, X., De Weireld, G., Frère, M., Giraudon, J.M., Leclercq, G., 2007b. Influence of the exchanged cation in Pd/BEA and Pd/FAU zeolites for catalytic oxidation of VOCs. Appl. Catal. B Environ. 70, 377–383, http://dx.doi.org/10.1016/j.apcatb.2006.02.027.
Todorova, S., Blin, J.L., Naydenov, A., Lebeau, B., Kolev, H., Gaudin, P., Dotzeva, A., Velinova, R., Filkova, D., Ivanova, I., Vidal, L., Michelin, L., Josien, L., Tenchev, K., 2019. Co 3 O 4 -MnO x oxides supported on SBA-15 for CO and VOCs oxidation. Catal. Today, 0–1, http://dx.doi.org/10.1016/j.cattod.2019.05.018.
Todorova, S., Blin, J.L., Naydenov, A., Lebeau, B., Karashanova, D., Kolev, H., Gaudin, P., Velinova, R., Vidal, L., Michelin, L., Josien, L., Filkova, D., Ivanova, I., Dotzeva, A., Tenchev, K., 2020. Co-Mn oxides supported on hierarchical macro-mesoporous silica for CO and VOCs oxidation. Catal. Today, 0–1, http://dx.doi.org/10.1016/j.cattod.2020.01.019.
Zabihi, M., Babajani, N., 2018. Modeling, optimization and experimental studies of supported nano-bimetallic catalyst for simultaneous total conversion of toluene and cyclohexane in air using a hybrid intelligent algorithm. RSC Adv. 8, 17346–17356, http://dx.doi.org/10.1039/c8ra01504j.

Zabihi, M., Khorasheh, F., Shayegan, J., 2015. Supported copper and cobalt oxides on activated carbon for simultaneous oxidation of toluene and cyclohexane in air. RSC Adv. 5, 5107–5122, http://dx.doi.org/10.1039/C4RA14430A.

Zhao, J., Tang, Z., Dong, F., Zhang, J., 2019. Controlled porous hollow Co3O4 polyhedral nanocages derived from metal-organic frameworks (MOFs) for toluene catalytic oxidation. Mol. Catal. 463, 77–86, http://dx.doi.org/10.1016/j.mcat.2018.10.020.

Zhao, Q., Zheng, Y., Song, C., Liu, Q., Ji, N., Ma, D., Lu, X., 2020. Novel monolithic catalysts derived from in-situ decoration of Co3O4 and hierarchical Co3O4@MnOx on Ni foam for VOC oxidation. Appl. Catal. B Environ. 265, http://dx.doi.org/10.1016/j.apcatb.2019.118552.

Zhuang, Y.Q., Gao, X., Zhu, Yping, Luo, Zhong, 2012. CFD modeling of methanol to olefins process in a fixed-bed reactor. Powder Technol. 221, 419–430, http://dx.doi.org/10.1016/j.powtec.2012.01.041.